ADVANCED FUNCTIONAL MATERIALS
www.afm-journal.de

Fast Electrodeposition of MXene/PDA Composites for High-Performance Bioelectronic Interfaces: An In Vitro Evaluation

Qi Zeng, Chenyang Xing, Zhen Xu, Qing Liu, Liangtao Yang, Hui Yang, Yi Zhang, and Zhengchun Peng**

Bioelectrode is critical to many biomedical researches. However, traditional materials (typically noble metals) and manufacturing techniques limit the large-scale production of bioelectrodes. Herein, a fast electrochemical approach is proposed to deposit versatile MXene/polydopamine (PDA) composites on a metalized substrate. PDA coating can improve the adhesion between MXene and the substrate, while MXene provides rough surfaces with unique micro/nanostructure and outstanding electrical/optical/thermal performance. The impedance of the as-prepared bioelectrode at 1 kHz is down to 8.48 Ω cm^2. The corresponding cathodic charge storage capacity (CSC_c) and charge injection capacity (CIC) are up to ≈250 and 6.59 mC cm^{-2} respectively, much superior to that of bare Pt and other conventional material-based electrodes. The MXene/PDA composites also demonstrate robust stability under continuous electrostimulation for 1 × 10^8 pulse cycles and 1000 CV cycles. Moreover, MXene/PDA composites show a high and rapid photothermal response. Photoelectrochemical activity is also observed with high photocurrent, ≈40 folds larger than that of bare Pt. The utility of this new electrode in ascorbic acid sensing is demonstrated. Excellent biocompatibility is verified via neuron adhesion test and viability assay.

1. Introduction

It is well-known that reliable bioelectronic devices have been proven promising for diverse applications, including biological applications such as health monitoring and clinical diagnosis/treatment, and related fields such as artificial intelligence and soft robotics, etc.[1–3] In this regard, there is an urgent need to develop multi-functionalized bioelectrodes within neuroscientific research for simultaneously detecting/recording the physiological parameters, biochemical assessments, and electrical/optical/thermal modulating or stimulating the targets, which are of great importance for digital healthcare.[4,5] Therefore, it is critical to explore suitable advanced biomaterials to perfectly realize the high-performance integration of bioelectronic devices.

Considering that the ideal bioelectronic interfaces usually require the bioelectrodes to meet the practical requirements of low interface impedance, excellent chronic stability, biological safety, etc., surface roughening and introducing bio-friendly nanomaterials to increase the effective surface area and the corresponding electrochemical performance are one of the commonly surface treatment strategies in recent years.[2] Importantly, nanostructured materials, due to their combination of high electrical conductivity and electromechanical flexibility, can effectively solve the challenges of electrode interfaces and even interact with biological systems at the molecular scale, to better serve the biomedicine-related fields. The traditional metal materials such as platinum (Pt), gold (Au), and iridium (Ir), carbon materials such as graphene and carbon nanotube (CNT), conductive hydrogels, and their hybrids have been researched extensively over the past few decades.[2,6–8] However, current technology still mainly depends on expensive materials and manufacturing solutions, and cannot achieve high volume and scale production, which seriously limits the practical applications.[2,9,10]

MXene, as a new family of 2D earlier transition-metal carbides and/or nitrides, has aroused extensive research interest since its discovery in 2011.[11] It has been reported that MXene exhibits a graphene-like nanostructure with a high specific surface area, hydrophilic surface with abundant functional groups, and unique metallic conductivity while having excellent mechanical, electrochemical, photothermal, and physical properties.[12,13] It was concentrated in the field of energy storage initially and gradually applied to gas, pH, glucose, and other biochemical sensing, as well as photothermal therapy and other biomedical fields due to those

Q. Zeng, C. Xing, Z. Peng
State Key Laboratory of Radio Frequency Heterogeneous Integration
School of Physics and Optoelectronic Engineering
Shenzhen University
Shenzhen 518061, China
E-mail: zcpeng@szu.edu.cn
Z. Xu, Q. Liu, L. Yang, H. Yang, Y. Zhang
Shenzhen Institute of Advanced Technology
Chinese Academy of Sciences
Shenzhen 518055, China
E-mail: yi.zhang3@siat.ac.cn
The ORCID identification number(s) for the author(s) of this article can be found under https://doi.org/10.1002/adfm.202312770

DOI: 10.1002/adfm.202312770

attractive merits.[14–23] Recently, it has been utilized for neural stimulation and recording successfully, showing great potential as a bioelectronic interface.[24,25] Whereas, in view of the low adhesion strength to the substrate, in most of the reported literature, MXene is usually chosen as one of the doping components, or as a conductive ink, and then processed into the required electrodes by means of drip coating, spin coating, printing, etc.[24–28] In addition, most reports on in situ deposition of MXene electrodes have focused on industrial applications such as electrocatalysis, where carbon materials are chosen as substrates due to their porosity and homogeneity. Since MXene nanosheets can form stable colloids in polar solvents because of high, negative zeta potential, electrophoretic deposition (EPD) has been considered an ideal and cost-effective approach to fabricate MXene-coated electrodes on conductive substrates.[29–31] Due to the advantages of excellent uniformity, large scale, mass production, and high deposition rate, EPD has also been applied to preparing silicon dioxide coating in silica sol in our previous work, showing excellent stability.[32] Yang et al. prepared binder-free titanium carbide (Ti_3C_2) MXene/carbon nanotubes (CNTs) films onto graphite paper via EPD at a high constant direct current (DC) voltage of 8 V for supercapacitor electrodes with enhanced electrochemical performance and excellent cycling stability, suggesting the feasibility of preparing MXene/CNTs films by simple EPD method.[33–34] It should be mentioned that current bioelectronic devices, especially most implantable electronics (e.g., retinal and cochlear prosthesis), use metal substrates and modification materials as conductors. The precious metal Pt, for example, is one of the most common materials in implants and has received United States Food and Drug Administration (FDA) approval.[2,35] To the best of our knowledge, in situ preparation of MXene-based bioelectrodes with well stability on metallic substrates is rarely reported. Huang et al.[36] utilized EPD to fabricate MXene-based bioelectrode on titanium (Ti) substrate, facilitating the antibacterial activity of the implants. However, the employed voltage was more than 30 V. It is still urgent to explore a mild in-situ preparation approach to achieve stable MXene-based bioelectrodes on metallic substrate for constructing functional bio-interfaces.

Considering that the introduction of an adhesive layer is one of the effective strategies to enhance electrode stability, which can be well-combined with other coating materials to obtain high-performance electrodes.[2] Therein dopamine (DA) is one of the bio-inspired molecules and can be polymerized onto different surfaces to form thick PDA coating for better bioelectronic interfaces with enhanced adhesion under practical conditions via strong hydrogen bonding and $\pi-\pi$ stacking interaction.[37–39] Most significantly, the groups (O—H, N—H) of the DA ring can form hydrogen bonds and originate —O from the catechol structure of PDA during the polymerization process,[40] therefore improving the hydrophilicity of the interface to some extent and promoting the chelation force of metallic ions, which has been verified and successfully fabricated on polymer substrate as an adhesive promoting layer for high-quality flexible electrodes in our previous work.[38,41] Herein, introducing a thin PDA film on the metallic substrate can be an effective strategy for the large-scale preparation of stable MXene-based bioelectrodes with enhanced interfacial properties.

To fulfill the requirements of bioelectronic interfaces in practical applications, we comprehensively consider the advantages of PDA and MXene, a facile two-step electrochemical micromachining route was proposed to develop versatile MXene/PDA composite bioelectrodes at room temperature and atmosphere pressure with low impedance, high charge storage capacity (CSC) and charge injection capacity (CIC), as well as good stability and biocompatibility. The PDA thin film was chosen as an adhesion layer and obtained by cyclic voltammetry (CV) deposition, followed by the MXene EPD process. Particularly, PDA provides at least two benefits: (a) providing an intermediate layer for MXene deposition with enhanced adhesion to metallic substrate; (b) the hydrophilicity of substrate can be improved appropriately, so as to facilitate the interface modification. A series of measurements were carried out to evaluate the versatility of MXene/PDA composites for bioelectronic interfaces including physical, electrochemical, photothermal, and photoelectric properties. Furthermore, stability and biosafety were also investigated concerning the long-term reliability of bioelectrodes.

2. Results and Discussion

2.1. Preparation and Characterization of MXene/PDA Composites

Generally, the surface state of the electrode is crucial for the performance of bioelectronics, therefore it is essential to ensure the effectiveness of electrode interface properties. **Figure 1** presents the electrodeposition process and mechanism of MXene/PDA composite coating. A variety of bare metallic materials can be employed as the conductive substrates in this experiment. In order to facilitae the subsequent comparison with the traditional neural electrodes, here the bare Pt electrodes were utilized as the substrates and proof of concept. After being carefully cleaned in acetone solution, the bare Pt electrodes were electrochemically conditioned in 0.5 M H_2SO_4 solution for more than 30 cycles in the range of −0.2 to 1.2 V (vs Ag/AgCl) at a scanning rate of 100 mV s^{-1} (Figure 1a). Subsequently, an intermediate PDA layer was introduced on the surface, where CV scanning was employed to promote the electropolymerization process. Particularly, the PDA layer is expected to promote good interfacial adhesion of MXene to Pt substrate and provide a relatively rough surface (Figure 1b). Subsequently, a secondary EPD of MXene film was conducted at a constant potential to finally afford to obtain functional MXene/PDA composites coated electrode. Notably, the MXene aqueous dispersion used in our experiment is relatively stable. There is still no condensation phenomenon after one month of storage, showing good stability (Figure S1, Supporting Information). Figure 1c shows the EPD setup i) and the corresponding schematic diagram of electrophoretic migration under a given electric field ii), respectively. The resultant force (F) subjected to MXene sheets can be expressed by the formula: $F = f_e - f_a - f_s$, where f_e stands for the electric field force that drives the negatively charged MXene sheets that gradually move to the anode, while f_a and f_s represent the interaction force and friction force on them during electrophoretic mobility, respectively.[32] More specifically,

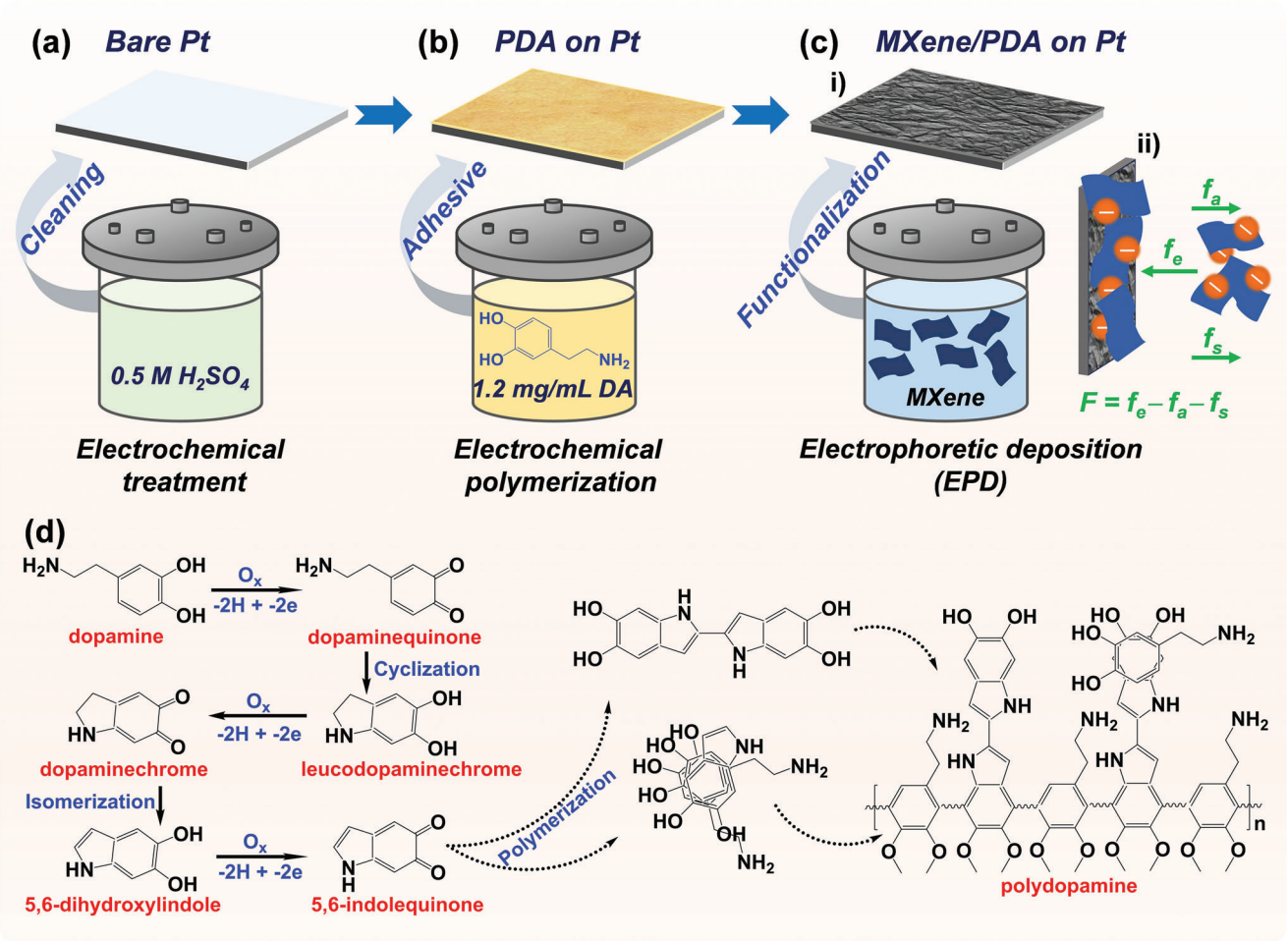

Figure 1. a–c) Schematic illustration for fast electrodeposition process of MXene/PDA composite electrode, including electrochemical treatment in 0.5 M H_2SO_4, electrochemical polymerization of 1.2 mg mL^{-1} DA in PBS, and electrophoretic deposition of 2 mg mL^{-1} MXene. The schematic diagram of MXene electrophoretic migration is shown in c–ii). d) Reaction mechanism on the electrochemical polymerization of PDA.

the EPD process of MXene can be expressed by the following formula:[34]

$$v = \frac{\sigma S_1 E}{k\eta\sqrt{S_r}} \quad (1)$$

where v is the drift velocity of the moving sheets. The upper half of the formula is the electric field driving force, σ is the surface charge density of MXene nanosheet, S_1 stands for the surface area and E is the strength of the electric field. k is the constant factor, η presents the viscosity coefficient, while S_r is the area of the flake's cross-section since most nanosheets move to the substrate in a vertical orientation under an electric field to reduce the floating resistance.

Nanosheets with larger effective diameters have a higher drift speed, which allows the larger nanosheets to preferentially deposit onto the substrate.[34] Therefore, the strength of the applied voltage, together with the concentration, uniform dispersion and stability of MXene aqueous dispersion are particularly important. Moreover, the reaction mechanism for the electropolymerization of PDA can be seen in Figure 1d. The initial step is the oxidation of catechol to quinone (O1), followed by cyclization. The next oxidation reaction is from leucodopaminechrome to dopaminechrome (O2). It should be mentioned that the highly crosslinked PDA films are composed not only of covalent bonds but also of supramolecular interactions.[37,42] Due to the low solubility of oxygen in water, the traditional polymerization process was time-consuming. When the solution pH is less than or equal to 7, it is challenging to obtain a PDA coating in a few hours.[38] In view of this fact, we utilized electrodeposition to quickly obtain the PDA intermediate adhesive layer and the second MXene layer in ≈1 h. The areal mass loading of each material in MXene/PDA composite coating after the deposition process can be calculated at 0.53 and 1.11 mg cm^{-2}, and their mass contents correspond to 32.49 and 67.51 wt.% (Figure S2, Supporting Information).

Figure 2a_1–d_1 show the optical images of different samples, including bare Pt, PDA, MXene, and MXene/PDA coated electrodes, respectively. As characterized by an atomic force microscope (AFM), the bare Pt electrode exhibits uniform distribution with a rather small root-mean-square (RMS) roughness of 1.79 nm (Figure 2a_2–a_4). The single PDA-coated electrode improves the surface in topology to some extent, also

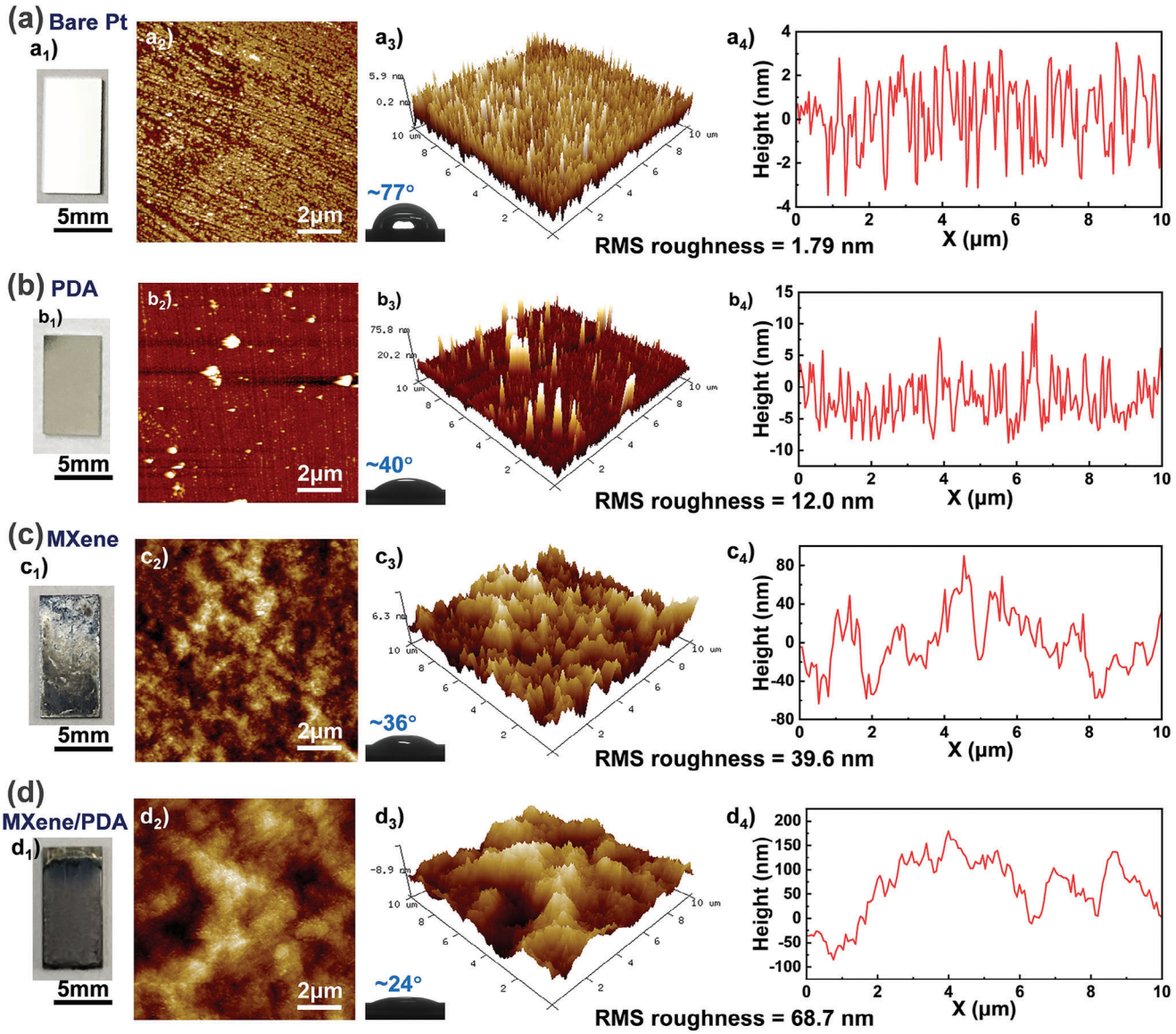

Figure 2. a_1–d_1) The optical images of bare Pt, PDA, MXene, and MXene/PDA coated electrodes, respectively. a_2–d_2) The representative topologic AFM images show high uniformity and increasing roughness. The inset presents the corresponding contact angle. a_3–d_3) 3D AFM images and a_4–d_4) the corresponding height profiles suggest the surface roughness of each layer (bare Pt, 1.79 nm), (PDA, 12.0 nm), (MXene, 39.6 nm), and (MXene/PDA, 68.7 nm).

presenting a relatively uniform distribution of 3D nanostructures without any undesirable cracks (Figure $2b_1$,b_2). The corresponding RMS roughness increases slightly to ≈12.0 nm, as shown in Figure $2b_3$–b_4. It should be mentioned that the single MXene material is difficult to adhere to the metal substrate uniformly without any intermediate adhesive layer (Figure $2c_1$). Nevertheless, we also tested the morphology of the comparatively homogeneous portion of the lower end of the sample. Particularly, the RMS roughness is found to increase dramatically to 39.6 nm (Figure $2c_2$–c_3), which can be attributed to the unique structure of MXene with an extensive contact interface. In order to prepare a uniform MXene interface, we introduced PDA as the intermediate adhesive layer and obtained MXene/PDA composite electrode. It can be seen from the optical image that the MXene layer is evenly coated on the surface of the PDA-modified electrode. The AFM results displayed in Figure $2d_2$–d_4 further clarify the uniform morphology with folded microstructure, resulting in a significant change in RMS up to 68.7 nm. Notably, introducing PDA on the electrode surface can significantly decrease the contact angle from ≈77° to ≈40°. Therefore, the MXene layer can better adhere to PDA modified surface with increased hydrophilicity (≈24° for MXene/PDA composites, ≈36° for single MXene coating), facilitating the interface modification (Figures $2a_2$–d_2). This inspiring phenomenon reveals that PDA coating improves the homogeneous dispersion of MXene deposition and its adhesion to the substrate, which is conducive to achieving higher performance of electrodes and also has far-reaching significance for the preparation

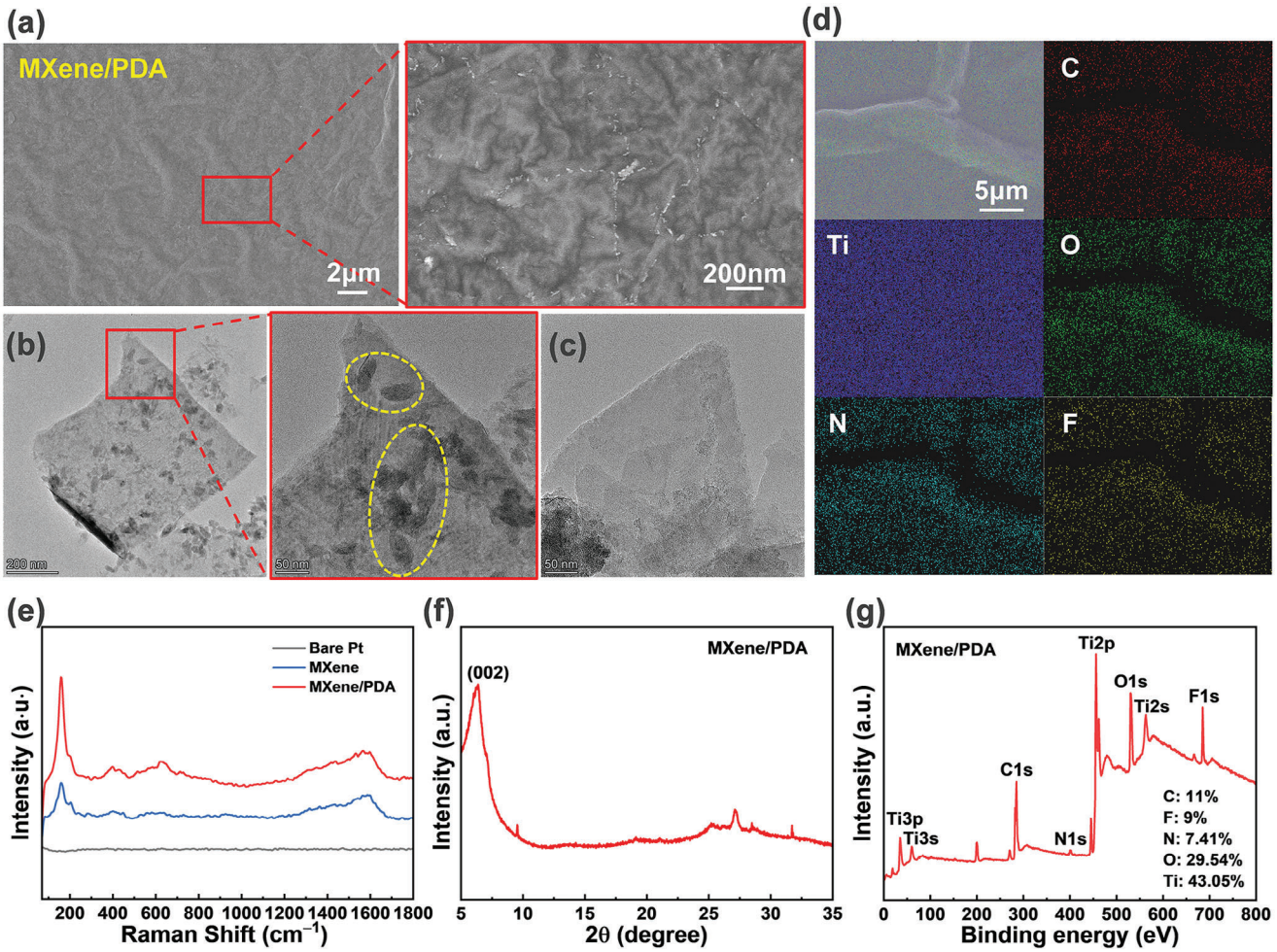

Figure 3. a) SEM images of MXene/PDA coated electrode. TEM images of b) MXene/PDA composites and c) MXene, respectively. d) SEM image and elemental (C, Ti, O, N, and F) mapping analysis of MXene/PDA coated electrode. e) Raman spectra, f) XRD patterns, and d) XPS survey spectra of the corresponding coated electrode.

of reliable bioelectronic devices and practical applications in the future.

Figure 3a shows the scanning electron microscope (SEM) images of MXene/PDA coated electrode, the uniform film has been evenly electrodeposited on the surface of the substrate via the electrodeposition method, and the folded microstructure can also be observed clearly in the enlarged area. This may be caused by the overlapping of nanosheets during electrodeposition, further increasing the roughness, which is consistent with the AFM data. Figures 3b,c display the transmission electron microscope (TEM) images of MXene/PDA and MXene after electrodeposition. It can be clearly seen the effective adhesion between PDA and MXene sheets, marked by the yellow circles in the enlarged area, demonstrating a visible difference from the pure MXene coating. In addition, the in-plane elemental mapping of the electrode was further obtained through energy disperse spectroscopy (EDS) (Figure 3d), which illustrates that MXene/PDA composites are comprised of C, Ti, O, N, and F elements, all are well distributed.

To further confirm the formation, surface composition, and electronic state of MXene/PDA composites, we obtained the Raman spectra, and X-ray diffraction (XRD) patterns and conducted X-ray photoelectron spectroscopy (XPS) analyses. The Raman spectroscopy results of bare Pt, MXene, and MXene/PDA composites were compared, displayed in Figure 3e. The rutile phase peaks at 398 and 612 cm^{-1} and the anatase phase peaks at 149 cm^{-1} demonstrating the formation of titanium dioxide.[43] The presence of the PDA intermediate layer accommodates more MXene coating on the substrate, thus promoting a stronger signal. The peaks at 198 cm^{-1} belong to the out-of-plane vibrations of Ti, C, and O atoms, while the wide peaks in the range 1200–1650 cm^{-1} are caused by the C—C bond formed by the oxidation of amorphous carbon.[44] As shown in Figure 3f, a strong intense peak of (002) plane is located at the low 2θ degree of 6.38°, which confirms the feasibility of preparing MXene composites by EPD. While there exists a shift toward lower 2θ for MXene/PDA compared to the pure MXene film as reported, illustrating the enhancement of d-spacing.[29,45] Figure 3g provides the broad spectrum of MXene/PDA-coated electrodes, similar to that reported in the literature.[30,46] The principal elements and atomic concentrations are 45.61% C, 7.87% F, 21% O, 2.22% N, and 23.3% Ti, respectively. It is worth mentioning that other metallic substrates,

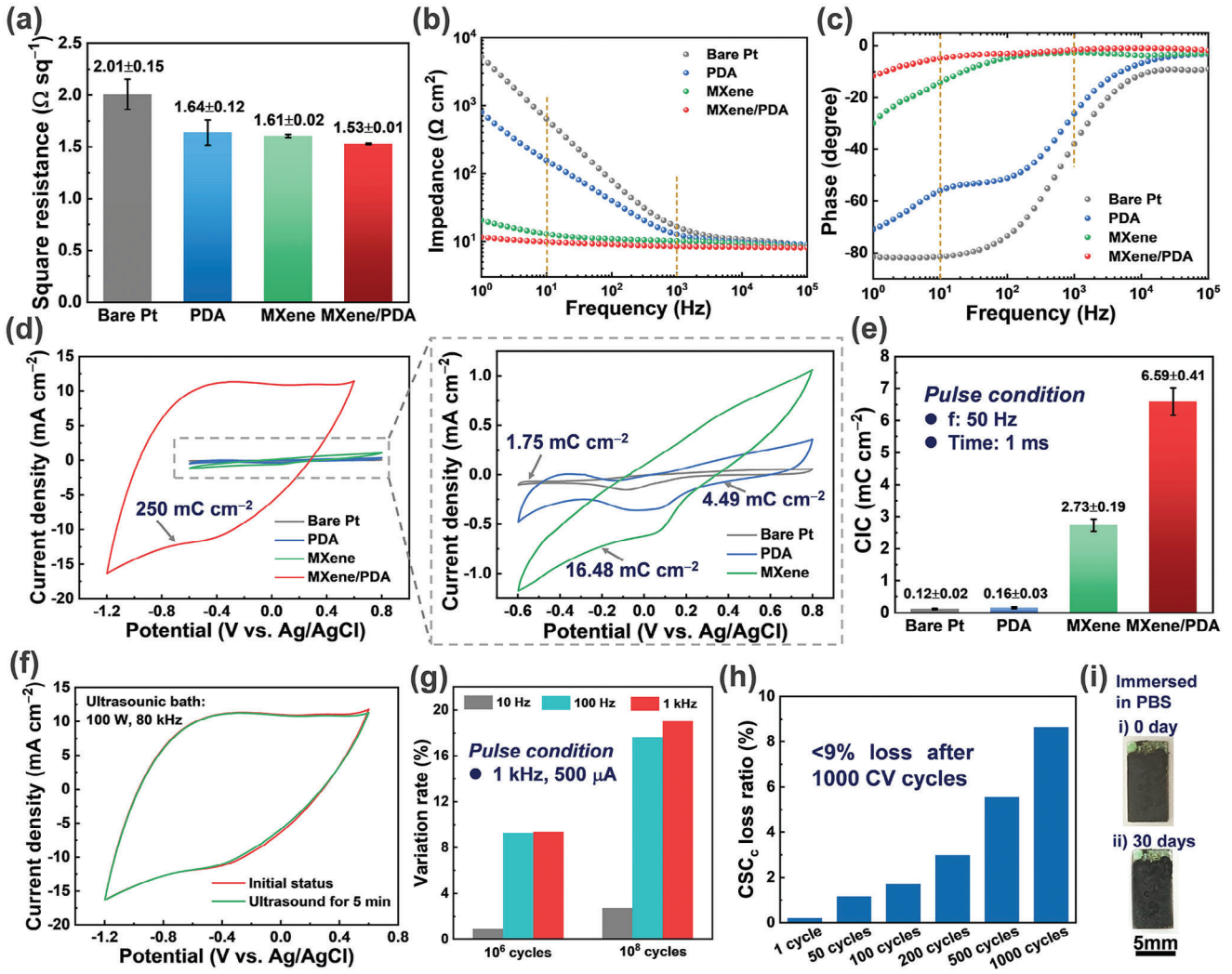

Figure 4. a) The comparison of square resistance of different electrodes (bare Pt, PDA, MXene, and MXene/PDA). b,c) EIS performances, including electrochemical impedance and phase angle, of bare Pt, PDA, MXene, and MXene/PDA coated electrodes in PBS. d) CV measurements and e) CIC performance of different coated electrodes. f) CVs of MXene/PDA coated electrodes before and after ultrasonic treatment. g) Variation rate of impedance at different frequencies after long-term electrical pulsing. h) CSC_c loss ratio of MXene/PDA coated electrode after different recycling CV scanning. i) Optical images of MXene/PDA coated electrodes before and after being soaked in PBS for 30 days.

such as Ti, stainless steel, zinc, magesium, etc., are also expected to be modified with MXene/PDA composites in a similar way for specific potential applications. These results amply verify the successful fabrication of MXene/PDA composite coating, which is beneficial for the subsequent functional testing of bioelectrodes.

2.2. Electrical and Electrochemical Properties

In order to investigate the potential application of MXene-based electrodes on neural interfaces, the electrical and electrochemical properties are critical to be evaluated before conducting implantation experiments. The four-probe test was carried out to investigate the electrical conductivity of prepared samples. It can be seen from **Figure** 4a that the square resistance of bare Pt electrode is 2.01 ± 0.15 Ω sq^{-1}, and subsequently decreases to 1.64 ± 0.12 Ω sq^{-1} (reduction of ≈18.41%), 1.61 ± 0.02 Ω sq^{-1} (reduction of ≈19.90%) and 1.53 ± 0.01 Ω sq^{-1} (reduction of ≈23.88%) after coated with PDA, MXene, and MXene/PDA composites, respectively, thus exhibiting the conductivity advantage for fabricating electronics.

To evaluate the electrochemical properties such as impedance and charge transfer ability of MXene/PDA electrodes, we conducted a series of electrochemical measurements under the physiological condition in phosphate buffer saline (PBS) in a three-electrode system, including electrochemical impedance spectroscopy (EIS), CV and charge pulsing experiments, to measure the impedance magnitude, CSC_c and CIC of each electrode. Figure 4b shows the electrochemical impedance of those modified electrodes in PBS at their open circuit potential. It can be seen that the electrochemical impedance of MXene/PDA electrode (8.48 Ω cm^2) at 1 kHz is reduced by 48.69%, 33.54%, and 16.54%, compared to that of bare Pt (16.53 Ω cm^2), PDA (12.76 Ω cm^2) and MXene (10.16 Ω cm^2) modified electrodes

respectively. While a more significant reduction of the impedance can be achieved at lower frequency. For instance, the impedance of the electrode at 10 Hz decreases from 639 Ω cm^2 (bare Pt) to 156.42 Ω cm^2 (PDA coating, reduction of 75.52%), 12.88 Ω cm^2 (MXene coating, reduction of 97.98%), and 9.85 Ω cm^2 (MXene/PDA composites, reduction of 98.46%) after modified with different materials respectively. The pronounced reduction can be attributed to the highly porous and rough morphology of modified electrodes with a high effective surface area at the interface. Notably, the increase in pseudo-capacitance of MXene can further reduce its impedance. Lower impedance means lower energy consumption will be required in practical applications to achieve the same stimulation/recording efficiency. Figure 4c represents the distinct variation of the phase angle following the PDA and MXene modification. At 1 kHz, the phase angle decreases from 37.85° (bare Pt) to 26.22° (PDA coating, reduction of 30.73%), 2.57° (MXene coating, reduction of 93.21%), and 1.63° (MXene/PDA composites, reduction of 95.69%) respectively. For 10 Hz, the corresponding phase angle varies from 81.5° (bare Pt) to 55.98° (PDA coating, reduction of 31.31%), 14.24° (MXene coating, reduction of 82.53%), and 4.79° (MXene/PDA composites, reduction of 94.12%) after modification, implying the enhanced charge transfer capacity of MXene-based electrode. It demonstrates that the decrement of interfacial impedance promotes the system approaching an ideal capacitance.[8] Moreover, the charge transfer impedance at the electrode interface is much lower, which is conducive to the effective reaction avoiding unnecessary losses.

The CV measurements for the electrodes within their respective water windows reveal a distinct increase in CSC_c for MXene-based electrodes, as shown in Figure 4d. The loop area of the bare Pt electrode is the smallest, with a minimum CSC_c of ≈1.75 mC cm^{-2}. While the CSC_c increases slightly to ≈4.49 mC cm^{-2} after being modified with PDA coating. A single MXene coating can improve the CSC_c of the electrode to 16.48 mC cm^{-2}. Inspiringly, the loop area of the CV curve under MXene/PDA modified electrode increases significantly, with the corresponding CSC_c reaching up to ≈250 mC cm^{-2}, which is ≈15.17, 55.68, and 142.86 times higher than that of MXene, PDA coated and bare Pt electrodes respectively. Such a high increment can be attributed both to the high effective surface area (ESA) and high intrinsic capacitance of MXene.[24] Meanwhile, the superior CSC performance will enable the electrode to store more energy in practical applications. CIC is another important parameter to evaluate the safe use of neural stimulation electrodes, which can be measured by increasing biphasic current pulses.[6,8] From Figure 4e, we can see that the MXene/PDA coated electrode substantially displayed the highest improvement of CIC up to 6.59 ± 0.41 mC cm^{-2}, compared with that of bare Pt (0.12 ± 0.02 mC cm^{-2}), PDA (0.16 ± 0.03 mC cm^{-2}) and MXene (2.73 ± 0.19 mC cm^{-2}) coated electrodes. Therefore, such high CIC will further reduce the stimulation potentials to achieve the desired efficiency under a tiny pulse current, actually minimizing the energy consumption within the safe voltage boundaries. Most importantly, applying PDA as an intermediate adhesion layer is able to enhance the electrical and electrochemical properties of MXene-based electrodes dramatically. We also verify that the proposed MXene/PDA coated electrode has good device-to-device stability through characterization and electrochemical testing of different samples, as shown in Figure S3 (Supporting Information).

The stability of neural electrodes is also essential for implantation applications since hundreds of millions of electrical pulse stimulations will be released on the electrode surface. First, a high-intensity ultrasound test (100 W, 80 kHz) was performed in PBS for 5 min to study the mechanical stability of MXene/PDA coated electrode, considering that ultrasonic treatment can easily remove the loosely attached substances on the surface. The CV variation curves shown in Figure 4f verify that the CSC_c value remains nearly unchanged (≈1.21% loss), implying excellent mechanical stability. Subsequently, we focused on the electrochemical stability of the MXene/PDA coated electrode, which was conducted in the three-electrode electrochemical cell. The impedance value of the electrode was evaluated in PBS after continuous electrical pulse stimulation at 1 kHz for different cycles. The corresponding variation rate is shown in Figure 4g. It can be seen that the impedance at 100 and 1 kHz increases by ≈9% after continuous stimulation for 1×10^6 cycles, while it only increases by ≈1% at 10 Hz low frequency. When we continued the stimulation process for up to 1×10^8 cycles, the impedance at 100 Hz and 1 kHz varied by ≈17.63% and 19.02%. Meanwhile, it increases slightly to ≈2.72% at 10 Hz, implying superior electrochemical durability. Thus, the designed bioelectrodes have significant advantages when a low-frequency stimulation is applied. Subsequently, CV scanning was also employed as the electrochemical stress to MXene/PDA. As shown in Figure 4h, only a minor change in CSC_c during the first 100 CV scans with less than 2% loss. It is thereby worth mentioning that the loss ratio of CSC_c is still less than 9% even after 1000 CV cycles, further indicating the stability of MXene/PDA coating in the electrical stimulation environment. In addition, the adhesion property of MXene/PDA coating was also studied by storing the electrode in PBS at room temperature for 30 days without any electrochemical stressing, compiled in Figure 4i. It can be seen that no obvious delamination occurred during the immersion since the coating kept nearly unchanged, further confirming the excellent stability. These inspiring results can be attributed to the strong chemical bonds formed between the interface of PDA coating and MXene layer. Thanks to the abundant amino and catechol groups, coating PDA as the intermediate layer provides more hydrogen bond binding sites on the surface including —OH group, $—NH_2$, and =O groups, facilitating the formation of abundant hydrogen bonding connections with —F and —OH groups on MXene sheets.[39,47,48] In addition, apart from the strong electrostatic interactions among PDA and MXene sheets, the catechol in PDA can also form coordination bonds with the edge Ti atoms, further improving the stability of the designed bioelectrodes.[49,50] **Table 1** demonstrates the comparison of the relevant parameters of MXene/PDA-coated electrodes with the typical neural electrodes reported in the literature. In addition to the reported traditional materials, the novel 2D MXene material provides a new strategy for developing next-generation high-performance neural interfaces.

It should be mentioned that our proposed MXene deposition method on metallic substrate demonstrates obvious advantages over other established methods such as drop-casting. As shown in Figure S4 (Supporting Information), EPD MXene/PDA composites present much superior electrochemical performance to

Table 1. Performance comparison of some typical materials for modifying neural electrodes.

Electrode materials	Geometric size [diameter]	Impedance at 1 kHz [Ω cm^2]	CSC_c [mC cm^{-2}]	CIC [mC cm^{-2}]	Stability	Reference
Bare Pt	0.3 cm^2	16.53	1.75	0.12	–	This work
Porous Pt	50 µm	0.33	Three times larger	4.4	–	[51]
Pt nanocone	200 µm	0.72	52.44	4.39	Impedance increases by ≈4.29%, CSC_c reduces by ≈23.07% after over 2 × 10^8 pulse cycles	[52]
Iridium oxide (IrO_x)	200 µm	1.19	66.88	3.19	Poor adhesion	[6]
Activated iridium oxide film (AIROF)	10 mm	15.25	58.57	–	<4% loss of CSC_c after 4 × 10^6 pulse cycles	[53]
Nanporous Au	30 µm	0.11	1	0.98	10% deviation of impedance after 60 min sonication	[54]
PDMAAp/PEDOT hydrogel	500 µm	–	128.76	3.7	<20% CSC loss after 1-year immersion in PBS	[5]
Poly(3,4-ethylenedioxythiophene): poly(styrenesulfonate) (PEDOT:PSS) hydrogel	–	10.09	82.36	–	No obvious change in CSC_c after 5 CV cycles	[55]
Carbon nanotube fiber (CNTF)	20 µm	0.88	278.21	3.52	–	[56]
MXene	3 mm	14.52	157.9	0.53	No change in impedance after suffering from 1000 cycles of 1.2-mA biphasic stimulation in PBS	[24]
MXene/PDA	0.3 cm^2	8.48	250	6.59	<9% CSC_c loss after 1000 CV cycles; impedance increases < 20% after stimulation for 1 × 10^8 cycles	This work

the coating obtained by drop casting. The impedance of the latter at 1 kHz and 10 Hz are ≈1.61 and 2.41 times higher than that of the former. While the CSC_c value of EPD MXene/PDA composites is 20 times higher than that of drop-coated samples. More seriously, after being immersed in PBS for 1 day, the drop-coated sample has a significant fall-off, implying low binding force and stability on the metallic substrate. For future work, it would be critical to optimize the electrode with well-controlled robust interfaces, which is essential for chronic implantation. One approach is to enhance the surface functionalization of MXene, and promote its strong adhesion to the substrate, thus achieving a high-stability bioelectronic interface.

2.3. Photothermal Properties

It has been reported that MXenes have outstanding photothermal performance under near-infrared (NIR) irradiation, which has been successfully applied to the optical controlling of neuronal electrical activity and the photothermal treatment of cancer without the need for supporting electrodes.[57,58] Hence, it is of great significance to investigate the photothermal-response performance of MXene/PDA-based electrodes for their future potential applications of photothermal stimulation in bioelectronic interfaces.

The schematic diagram of the experimental set-up for investigating the photothermal behaviors is illustrated in **Figure 5a**. For experimental testing, an 808 nm NIR laser was provided as an excitation light source and the temperature variation of the sample was recorded instantaneously using a real-time IR thermal imaging camera. As shown in Figure 5b, the temperature of single bare Pt and PDA-coated electrodes rises slowly to 30.1 and 32.8 °C respectively within 60 s under continuous irradiation with a power density of 2 W cm^{-2}. In contrast, the single MXene-coated electrode exhibits an obvious photothermal-response behavior, reaching a high temperature of up to 110 °C under the same conditions. The MXene/PDA composites coated electrode presents a much higher photothermal-response with an ultrahigh surface temperature up to 160 °C, indicating that the enhanced photothermal-response performance is well retained in MXene-based composites. Note that the temperature increases approximately linearly during the first 10 s, as displayed in Figure 5c. It can be seen that MXene/PDA composite demonstrates the highest heating rate of ≈7.12 °C s^{-1}, which is ≈1.94, 13.69, and 18.26 times higher than that of pure MXene (3.67 °C s^{-1}), PDA (0.52 °C s^{-1}), and bare Pt (0.39 °C s^{-1}) electrodes respectively. This should be attributed to that the PDA intermediate layer with a certain roughness can effectively accommodate more MXene without falling off. As shown in Figure S5 (Supporting Information), there is no obvious change in the macroscopic image of the coating. The corresponding microstructure before and after the photothermal reaction also demonstrates no significant differences, displayed in the optical and SEM images. Furthermore, the fast local heating caused by MXene under NIR laser irradiation, as well as the synergistic promotion of PDA, promote the rapid photothermal responses.[44] Subsequently, we compared the photothermal performance of MXene/PDA coated electrodes under different NIR laser power densities (0.25–1.5 W cm^{-2}), and the insets display the corresponding thermal images obtained by an IR camera (Figure 5d). The laser power was gradually increased

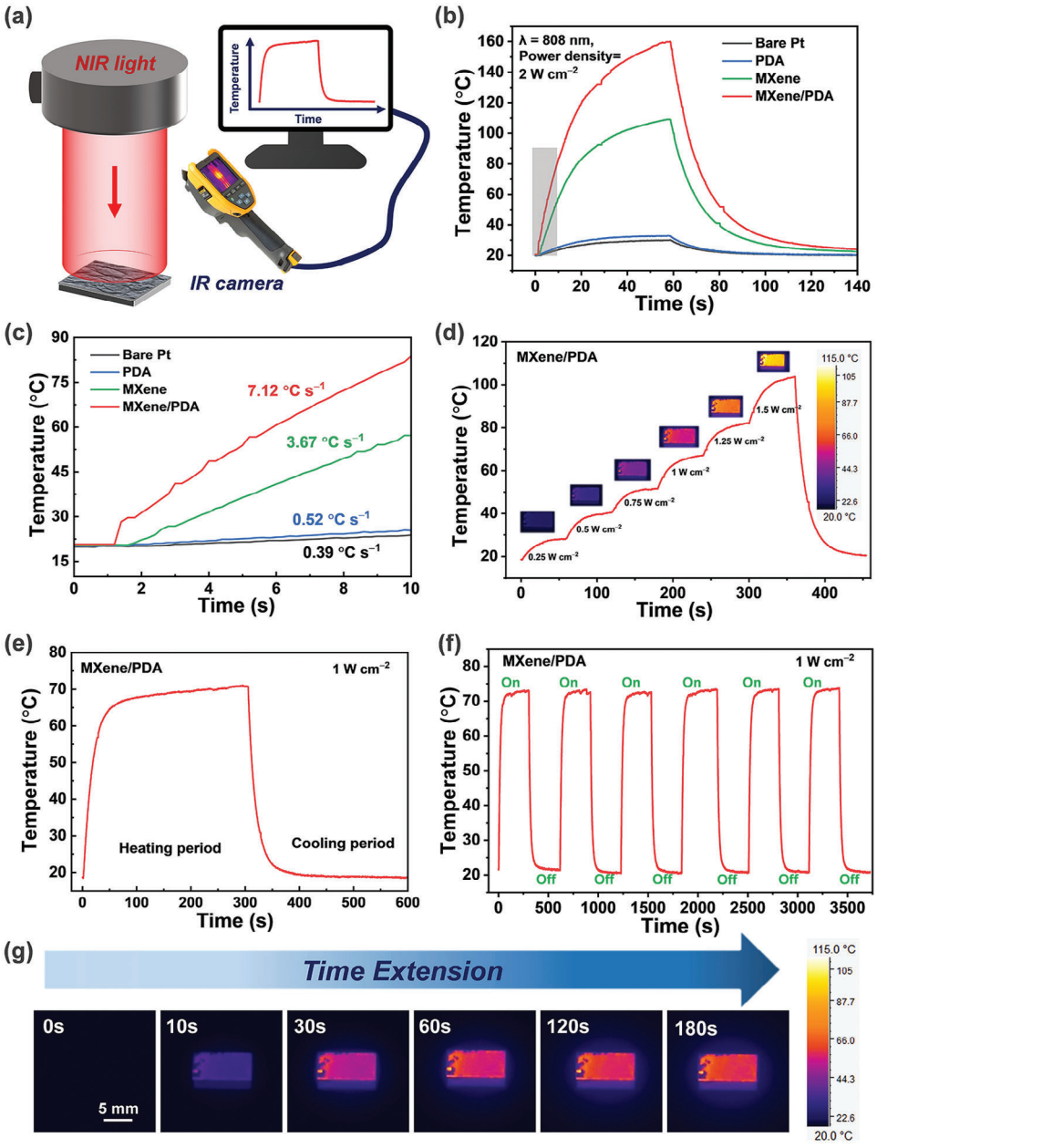

Figure 5. a) The schematic diagram of the experimental set-up for investigating the photothermal behaviors of different coated electrodes. b) Photothermal heating curves of bare Pt, PDA, MXene, MXene/PDA coated electrodes under the irradiation of an 808 nm NIR laser at a 2 W cm^{-2} power density. c) Comparison of the linear curve of temperature rise in the first 10 s. d) Temperature profiles of MXene/PDA coated electrode under a stepwise NIR laser power density of 0.25–1.5 W cm^{-2}. The insets show the corresponding photothermal images. e) The temperature increase and decrease of the MXene/PDA coated electrode with laser illumination for 300 s and light off, respectively. f) Temperature–time curve of MXene/PDA coated electrode for six laser on/off cycles. g) Infrared thermographic photographs of MXene/PDA coated electrodes under NIR irradiation at different time intervals.

every 60 s. The surface temperature of the composite electrode reaches ≈28.4 °C at the first 60 s under continuous NIR laser irradiation at a low power density of 0.25 W cm^{-2}. Moreover, an enhanced power density of 0.5 W cm^{-2} yields a higher temperature of ≈40.6 °C, which further increases to 51.6, 67.1, 81.9, and 103.8 °C at 0.75, 1, 1.25, and 1.5 W cm^{-2}, respectively, reflecting a significantly increased photothermal performance with the elevation of NIR power. Furthermore, the composite electrode demonstrates a fast cooling-down process once turning off the light source.

In view of the photothermal stability under NIR light irradiation, we increased the illumination time to 5 min. As illustrated in Figure 5e, taking a power density of 1 W cm^{-2} as an example, MXene/PDA coated electrode rapidly reaches the equilibrium temperature of ≈70 °C when a balance is achieved between the environment-absorbed energy and the light-induced thermal

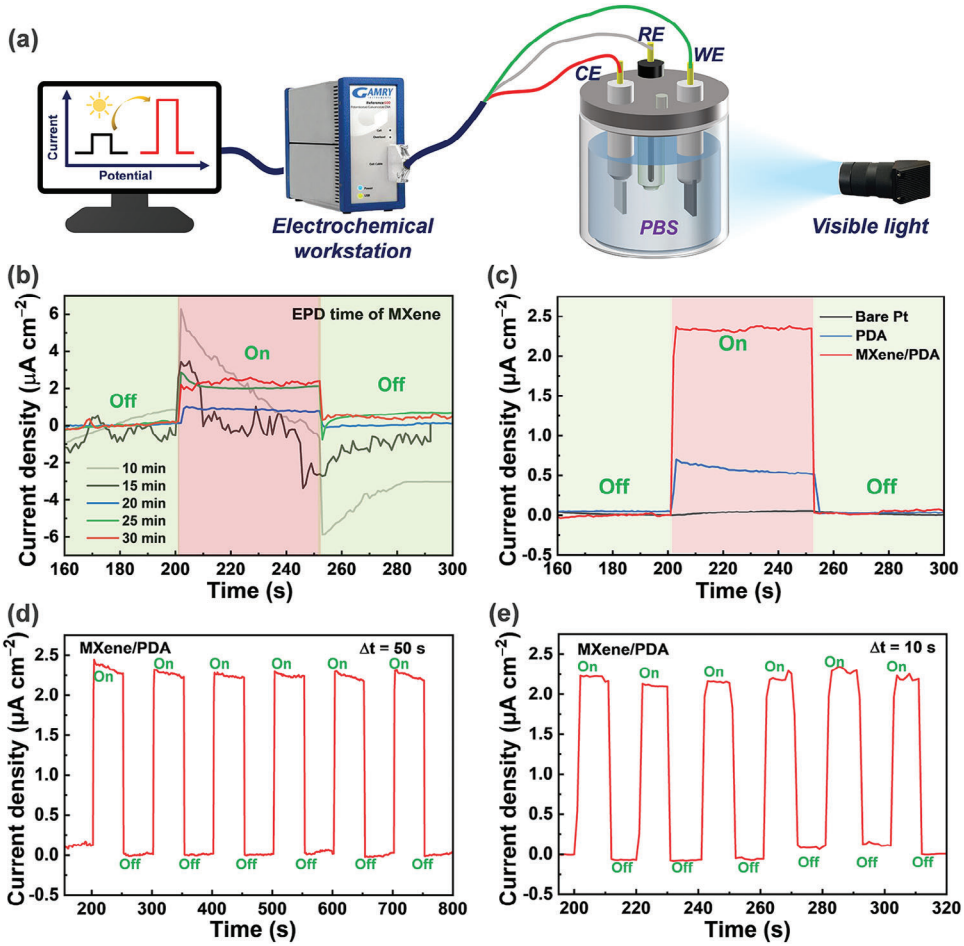

Figure 6. a) The schematic diagram of the photoelectrochemical performance measurements process. b) Photocurrent response in PBS of MXene/PDA coated electrodes under different EPD times. c) Photocurrent response of bare Pt, PDA, and MXene/PDA coated electrodes. d,e) Photocurrent response curves of MXene/PDA coated electrode over varying intervals of time (Δt: 10–50 s) for six laser on/off cycles.

energy after exposing the electrode to continuous NIR light irradiation for ≈3 min. The recycling temperature variation in MXene/PDA coated electrode was carried out under NIR irradiation for 5 min (light on) followed by natural cooling to ambient temperature (light off) for six on/off light cycles to further investigate the photothermal stability. It can be seen from Figure 5f that the photothermal performance of MXene/PDA coated electrode shows no obvious deterioration during the whole cycling process, conforming to the superior photothermal stability. Meanwhile, the photothermal stability of different batches has been further verified by testing three different samples (Figure S6, Supporting Information), and the results showed no significant difference. Figure 5g shows the corresponding infrared thermographic images of the surface temperature during the heating process. The temperature increases drastically from 18.7 to 36.7 °C in 10 s and to 68.1 °C in 120 s, and then gradually becomes stable, implying a rapid heating process due to the excellent photothermal performance of MXene. These results reveal the possibilities for MXene/PDA coated electrodes and may provide a positive promotion effect for future bioelectronic devices and interfaces in photothermal therapy, photothermal stimulation, and other potential applications. Additionally, more work is still needed to develop optimized MXene-based electrodes with lower incident energy densities to achieve a more desirable stimulation effect.

2.4. Photoelectrochemical Properties

2.4.1. Photoelectrochemical Response

In addition to the above excellent properties, it is also of great significance to investigate the photoelectrochemical properties of MXene-based electrodes for bioelectronic applications in the future, including recording nerve signals, cell activity, etc.[57,59] The schematic diagram of the photoelectrochemical performance measurements process is shown in **Figure 6**a. To achieve a stable photocurrent response, we initially compared different MXene electrodes by varying the EPD time. As displayed in Figure 6b, the transient photocurrent response (*I*–*t* curve) is unstable when EPD time is less than 15 min. This may be due to the short EPD time, which leads to the failure of MXene coating to uniformly cover the electrode surface. However, with the increase of the

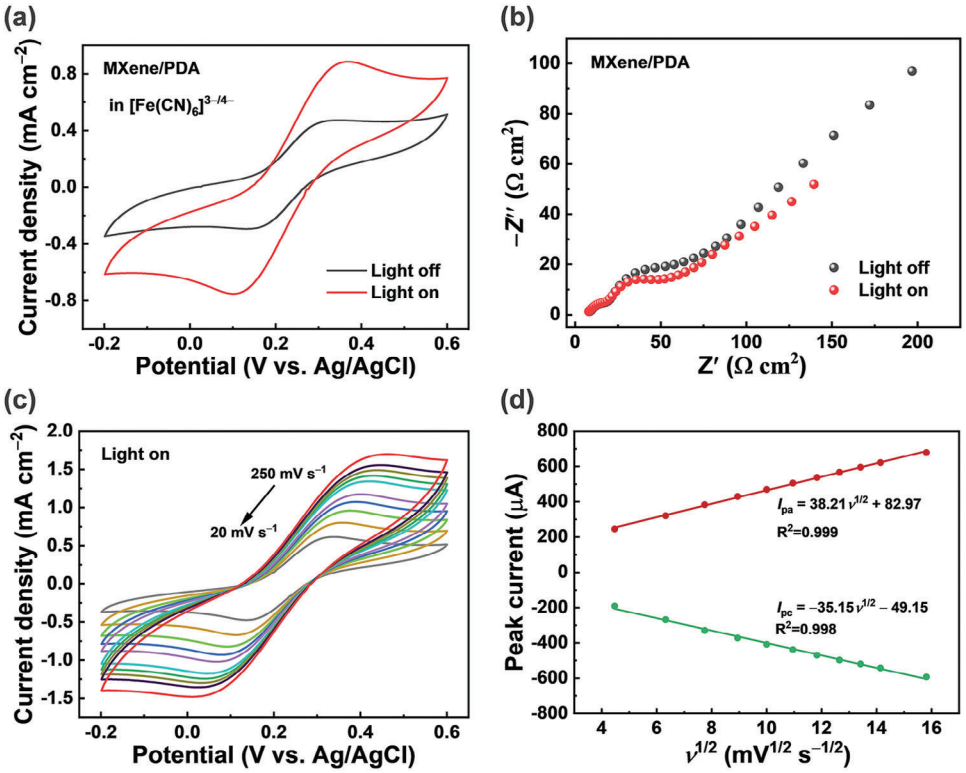

Figure 7. a) CV and b) Nyquist plots of MXene/PDA coated electrode measured without and with visible light in 0.1 KCl + 10 mM $K_3[Fe(CN)_6]/K_4[Fe(CN)_6]$ solution under open circuit potential. c) CVs of MXene/PDA coated electrode at scan rates from 20 to 250 mV s^{-1}. d) Linear relationships between anodic/cathodic peaks currents and the square root of the scan rate.

EPD time, the photocurrent response tends to stabilize, which is conducive to our subsequent research.

Figure 6c shows the photocurrent response of bare Pt, PDA coating, and MXene/PDA composites, respectively. It is noted that bare Pt exhibits a weak photocurrent response (≈0.05 μA cm^{-2}). The photocurrent intensity of MXene/PDA composites reaches ≈2.32 μA cm^{-2}, namely ≈4.14-flods and 46.4-folds larger than that of PDA coated electrode (≈0.56 μA cm^{-2}) and bare Pt electrode respectively. Such sensitive photocurrent response clarifies the superior and more efficient charge separation and transport capacity, which can be attributed to the effective transference of photoelectrons from the substrate to MXene modification layer.[60] Meanwhile, the rapid photocurrent response from the photoelectrode at the "on-off" moment of the irradiated light source further indicates that the MXene/PDA modified electrode can realize the rapid excitation, separation, and transfer of charge under light excitation. Importantly, the MXene/PDA modified electrode exhibits a repeatable photocurrent response over varying intervals of time (Δt: 10–50s), with no significant change under six repeated light "on-off" cycles (Figure 6d,e), indicating that the prepared photoelectrode has good signal output stability. Most significantly, the photocurrent density remains almost unchanged when continuous illumination reaches ≈10 000 s (Figure S7, Supporting Information), therefore the MXene/PDA electrode/solution interface exhibits exceptionally excellent photoelectrochemical stability.

2.4.2. Electrode Activity Toward Physiological Detection

Based on the above research, we further employed the prepared MXene/PDA composites as the photoactive electrode material to construct the photoelectric biochemical sensor. The electrochemical activity of MXene/PDA-modified electrodes was studied in a solution containing 10 mM $K_3[Fe(CN)_6]/K_4[Fe(CN)_6]$ and 0.1 M KCl under open circuit potential at a scanning rate of 50 mV s^{-1}. **Figure** 7a shows a pair of well-defined reversible REDOX peaks in the CV curves. In general, the higher REDOX peak current indicates excellent conductivity.[61,62] The EPD process results in the addition of oxygen-containing functional groups in MXene nanosheets, which will produce more active sites for electrochemical reactions.[63] Due to the excellent conductivity of MXene, the prepared electrode displays a high redox peak current. More importantly, when visible light was applied, the redox peak current of MXene/PDA electrode increased significantly compared with that under no light irradiation, indicating that applying visible light is conducive to improving the conductivity of MXene/PDA modified electrode. Moreover, the cathodic to anodic peak current ratios (I_{pc}/I_{pa}) of the electrode under light irradiation is revealed to be ≈1.07, implying that MXene/PDA-modified electrode exhibits excellent reversible activity. Actually, MXene can capture photo-excited electrons effectively and promote the separation of electron/hole pairs, therefore enhancing electrical conductivity.[62] Furthermore, EIS measurement was carried out to explore the carrier recombination/transfer

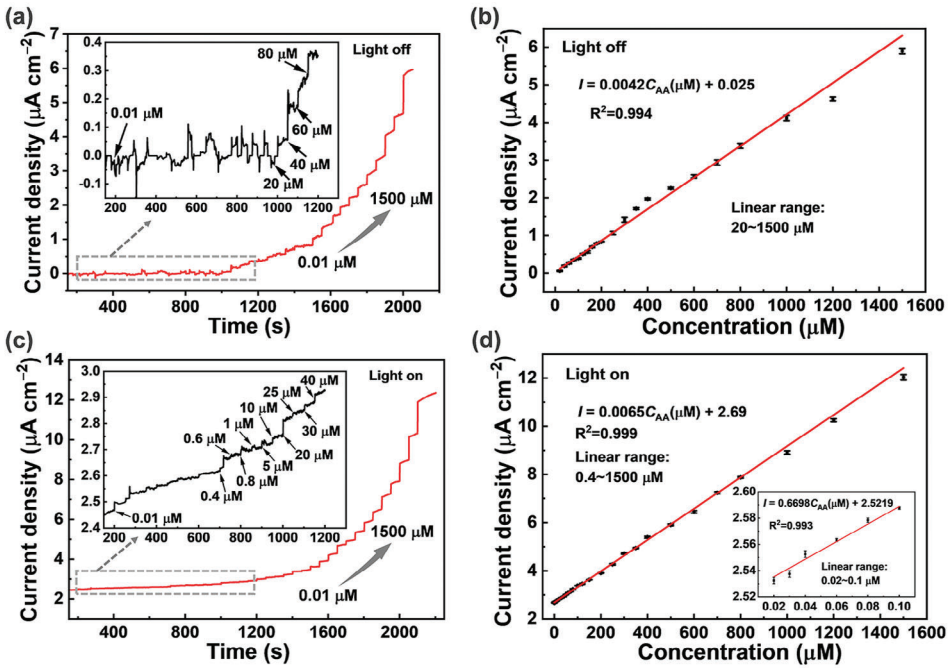

Figure 8. Current–time curves of MXene/PDA coated electrode with different concentrations of AA a) without and (c) with light irradiation. (b) and (c) are the corresponding linear calibration curves respectively.

behavior of the as-prepared electrodes, depicted in Figure 7b. It can be seen that the arc size of the Nyquist curve with visible-light illumination is much smaller than that without light, suggesting that the visible light irradiation can efficaciously promote the interfacial charge transfer rate at the interface of MXene/PDA-modified electrode, and thereby improve the photoelectrochemical properties.[60] This result is consistent with that of I–t curve test for photoelectrochemical response. The MXene modification may prevent the excessive charge accumulation on the bare Pt electrode surface, and improve the response to visible light. Thus, the introduction of MXene and visible light is conducive to improving the electrochemical performance of bare Pt electrodes.

In addition, CV was also performed to measure the electrochemical behavior of MXene/PDA-modified electrodes at scan rates ranging from 20 to 250 mV s^{-1}, as presented in Figure 7c. It can be seen that both the cathodic peak current (I_{pc}) and anodic peak current (I_{pa}) increase with a positive potential displacement as the scan rate increases. Figure 7d shows the well-fitted linear relationships of the oxidation and reduction peaks currents, with the square root of scan rates, indicating that the electrochemical process at the surface of MXene/PDA modified electrodes is controlled by diffusion.[64]

2.4.3. Determination of Ascorbic Acid Detection Sensitivity

In order to demonstrate the applicability as photoelectrochemical biosensor devices, the MXene/PDA-modified electrodes were utilized as a proof of concept for detecting ascorbic acid (AA), considering that AA is one of the most important neurochemicals in the brain and plays an important neuroprotective and neuromodulatory role in brain dysfunction/injury.[65] Current–time (I–t) curve was selected to explore the stepwise process for quantitative measurement of AA, from which the appropriate detection range and the limit of detection can be achieved. **Figure** 8a shows the continuous current response for varied concentrations of AA (0.01–1500 μM) at intervals of 50 s in the presence of PBS solution, without light irradiation applied to the test system. The current response was recorded for each addition of AA. When the concentration is below 20 μM, the current signal is quite unstable. While it increases linearly from 20 to 1500 μM, as displayed in Figure 8b. The corresponding linear regression equation can be described as I (μA cm^{-2}) = 0.0042 C_{AA} (μM) + 0.025 (R^2 = 0.994). The limit of detection (LOD) of AA is crucial for the practical application and it is calculated to be 3.14 μM. To be mentioned, a fast and stable response can be observed under light irradiation. The MXene/PDA modified electrode can achieve a much wider linear response range (0.02–0.1, 0.1–0.4, and 0.4–1500 μM). The linear fitting results can be presented as I_1 (μA cm^{-2}) = 0.6698 C_{AA} (μM) + 2.5212 (R^2 = 0.993, 0.02–0.1 μM), I_2 (μA cm^{-2}) = 0.2181 C_{AA} (μM) + 2.5638 (R^2 = 0.949, 0.1–0.4 μM), and I_3 (μA cm^{-2}) = 0.0065 C_{AA} (μM) + 2.69 (R^2 = 0.999, 0.4–1500 μM). Particularly, the electrode can achieve a much lower LOD of 0.0045 μM with nearly a three-order-magnitude winder linear range than that without light irradiation, demonstrating the superior photoelectrochemical detection potential (Figure 8c,d). Most importantly, the catalytic material on the surface of the working electrode can be "activated" in the electric field, and AA will be adsorbed to the active sites of the catalytic active material and quickly oxidized to dehydroascorbic acid. Subsequently, dehydroascorbic acid will be released from the catalytic active material due to diffusion. The electrical signal can be generated during the reaction process, therefore the photoelectrochemical properties of modified materials on the working electrodes will significantly affect its

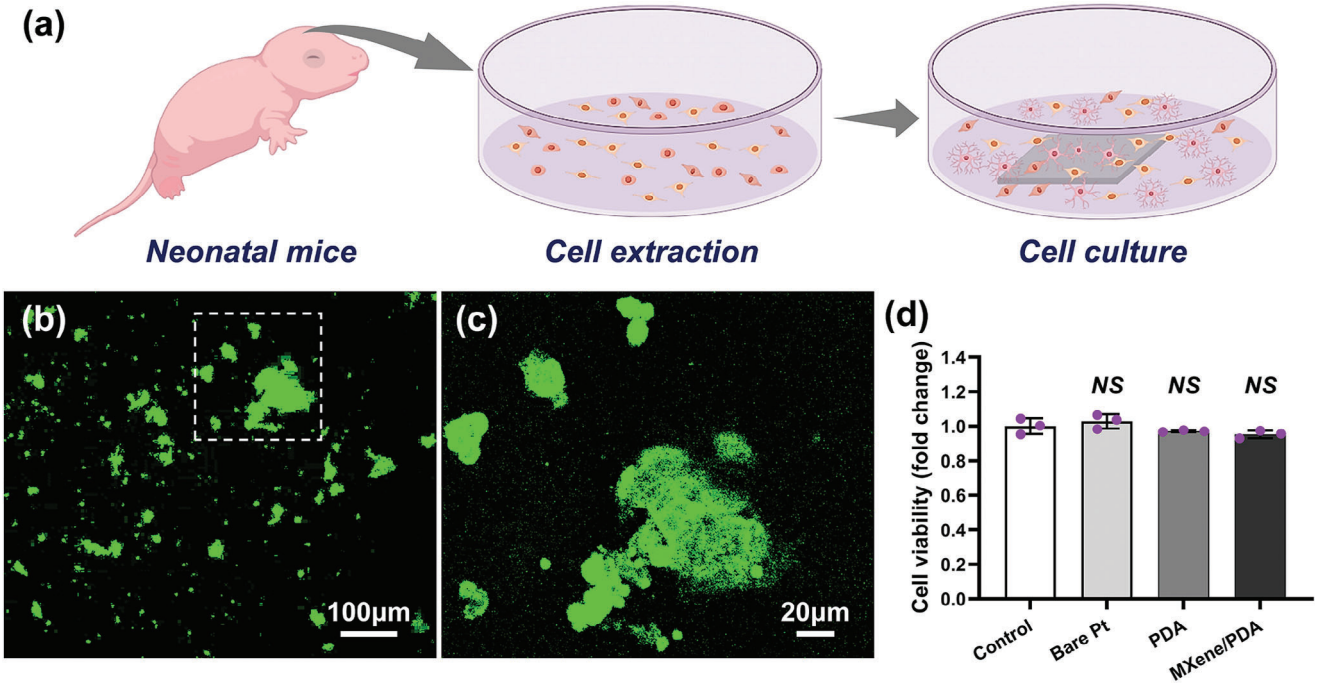

Figure 9. Biocompatibility evaluation of the designed electrodes on primary mouse neurons. a) Schematic diagram of neuron cell extraction from the neonatal mice, and co-culture on electrodes. b,c) Fluorescent images showing neurons cultured on MXene/PDA coated electrode after 24 h. d) Quantification of neuron viability following culture with the indicated electrode extracts using CCK8 viability assay. NS denotes not significant.

sensing performance.[65,66] Moreover, the selectivity test using the MXene/PDA-coated electrode was also performed. As observed in Figure S8 (Supporting Information), the response signals of uric acid (UA, 25 μM), glucose (25 μM), and KCl (25 μM) were negligible for AA detection, exhibiting good selectivity. In the future, we will deeply explore its detection mechanism and systematically study its specificity, anti-interference, and stability, so as to further extend to multi-parameter real-time monitoring in implantable/wearable environments.

2.5. Biocompatibility Study

Minimizing the potential cytotoxicity and foreign body response is critical to achieving long-term reliable bioelectronic interfaces, especially for implantable devices. Here, to assess the biocompatibility of the designed electrodes before being applied in vivo, we tested the effect of bare Pt, PDA, and MXene/PDA composite on the adhesion and viability of in vitro cultured primary mouse neurons. **Figure** 9a displays the schematic diagram of neuron cell extraction from the neonatal mice, and co-culture on electrodes.

For neuron adhesion, the neurons were plated on the surface of MXene/PDA composite electrode. The fluorescence micrographs displayed in Figure 9b,c clearly show the good neuron adhesion on MXene/PDA composite electrode. In addition, after culturing with different electrode extracts, a CCK8 viability assay was performed to determine the effects of different electrode extracts on neuron viability. It can be seen from Figure 9d that bare Pt, PDA, and MXene/PDA extracts show no difference in neuron viability. Consequently, our designed MXene-based bioelectrode possesses good biocompatibility with neurons, which has an important role in promoting future implantable research.

3. Conclusion

In this study, we developed a facile two-step electrochemical micromachining technique to fabricate high-performance MXene/PDA composite-based bioelectrodes at room temperature and atmosphere pressure. First, a thin PDA layer was prepared on the metallic substrate by a simple CV electropolymerization. Subsequently, MXene with functional groups was deposited via an EPD process under constant potential. The resulting composite electrode has a very low electrochemical impedance down to 8.48 Ω cm^2 at 1 kHz. It also exhibits a high CSC_c and CIC up to ≈250 and 6.59 mC cm^{-2}, which are ≈142.86 and 41.19 times higher than that of bare Pt electrode, respectively. The MXene/PDA electrode also shows robust stability under continuous electrostimulation for 1×10^8 pulse cycles and 1000 CV cycles. Importantly, the MXene/PDA composite presents a high and fast photothermal response under NIR laser irradiation. In addition, it shows excellent photoelectrochemical activity with a photocurrent 40 folds larger than that of bare Pt. As a proof of concept, we utilized the MXene/PDA electrodes to detect ascorbic acid with a low LOD of 4.5 nM. This result reveals that light irradiation can efficaciously promote electron transfer across the electrode materials and thereby improve the photoelectric sensing performance.

Due to the excellent biocompatibility, our bioelectrodes also hold promise for alleviating neurological complications, which is attractive for implantable and other biomedical applications. Future studies should be directed toward investigating the electrophysiological performance and long-term stability both in vitro

and in vivo. Different stimulation/regulation strategies can be supplemented and combined to evaluate other performances of these electrodes. Most significantly, the proposed MXene-based bioelectrodes have much-reduced cost, which is promising for new-generation bioelectronic interfaces in both research and clinical applications.

4. Experimental Section

Preparation of MXene/PDA Composite Electrode: The platinized silicon (Si) wafer (5 mm × 10 mm) was utilized as the conductive substrate. The MXene/PDA nanocomposites were electrodeposited using a three-electrode electrochemical setup. For the two layers, the PDA coating was applied as an adhesion layer between Pt substrate and MXene, while the second functional MXene layer was used to contact with the target medium directly. A Gamry Reference 600 electrochemical workstation was employed for all the electrochemical experiments. The modified electrodes (exposed area: 5 mm × 5 mm) were thereby connected as the working electrode (WE), and a large Pt sheet and an Ag/AgCl electrode were used as the counter (CE) and reference electrodes (RF), respectively. Prior to the experiments, all the samples were carefully cleaned in acetone solution, and electrochemical conditioned in 0.5 M H_2SO_4 solution.

The first layer of PDA was electropolymerized with a DA precursor solution (1.2 mg mL^{-1} dopamine hydrochloride (DA-HCl, powder), purchased from Aladdin). Phosphate-buffered saline (PBS) was used as the solvent, purchased from ThermoFisher. The freshly prepared solution was transparent and the pH was measured at ≈7.4. The PDA layer was then electropolymerized on Pt substrate at a slow rate of 50 mV s^{-1} CV scanning between −0.5 and 0.5 V (vs Ag/AgCl) for at least 60 cycles.

The second MXene layer was achieved in a uniform suspension containing 2 mg mL^{-1} MXene (purchased from Foshan Xinxi Technology Co., LTD) using deionized water as the solvent, which was performed at a constant potential of 3 V for 20 min via EPD. The distance between the working electrode and the counter electrode is ≈1 cm in all the electrochemical experiments. Consequently, a black coating was obtained and dried at room temperature for more than 12 h.

Material Characterizations: An atomic force microscope (AFM, NanoManVS, Germany) was applied to measure the 3D morphology and root-mean-square (RMS) roughness of the as-fabricated samples. The field emission scanning electron microscopy (FESEM, Zeiss SIGMA 300, Germany) was employed to analyze the surface morphology and microstructures, while the corresponding energy dispersive spectrometer (EDS) was used to analyze the elements of MXene/PDA composites. The transmission electron microscopy (TEM) images were taken on the transmission electron microscope (FEI Talos F200x, USA). Raman spectra were performed by LabRam HR Evolution (WITec alpha300R, Germany) under an excitation wavelength of 532 nm. The crystalline structures of MXene/PDA composites were characterized by an X-ray diffractometer (XRD, Rigaku SmarLab SE, Japan) at a scan rate of 2°min^{-1} with Cu Kα radiation. The XRD measurements were performed with an acceleration voltage at 40 kV and 50 mA current to record data in a range of 2θ of 5–90°. The corresponding compositional analysis and bond energy were analyzed by an X-ray photoelectron spectroscopy (XPS, Thermo Scientific K-Alpha, USA) with Al Kα radiation (hν = 1486.6 eV, 12 kV, 6 mA).

Electrical and Electrochemical Measurements: The electrical and electrochemical characteristics of MXene/PDA modified electrodes, together with PDA and bare Pt electrodes, were assessed by a range of measurements, including a four-point probe, electrochemical impedance spectroscopy (EIS), cyclic voltammetry (CV), and pulse-testing.

The multifunction digital four-probe tester (ST-2258C, Suzhou lattice Electronics Co., LTD) was used to measure the square resistance of the samples so as to evaluate their electrical conductivity preliminarily. All the electrochemical measurements were performed in PBS solution at room temperature in the same three-electrode setup as described in Section 2.1. EIS tests were conducted from 100 kHz to 1 Hz with a 10 mV amplitude signal. CV sweeps were obtained within the electrodes between potential limits of −0.6 and 0.8 V at a scan rate of 50 mV s^{-1}, which was utilized to determine the cathodic charge storage capacity (CSC_c, defined as the cathodic area enclosed with one CV cycle). Prior to the tests, all the samples were soaked in PBS for ≈30 min to stabilize the electrode in solution.

Puls-testing was employed to evaluate the maximum CIC of the electrodes, which can be conducted with a neural stimulator (PENS0410, Greentek, China) to provide a symmetric biphasic current pulse (1 ms pulse width, 50 Hz) between the working electrode and counter electrode. Meanwhile, a digital oscilloscope (TPS2012B, Tektronix, China) was applied to record the potential excursion between the working electrodes and the reference electrode. The maximum CIC can be achieved when the measured potential reaches either side of the safe potential window, after subtracting the ohmic voltage drop ("*IR* drop").[7]

Stability Evaluation: The mechanical stability of the as-fabricated bioelectrodes was estimated in PBS by applying an intensive ultrasonic bath (100 W, 80 kHz) for 5 min. The corresponding CSC_c variation of electrodes was then observed after being stabilized in PBS for 30 min.

The electrochemical stability was examined by applying a long-time pulsing with continuous cathodic-first biphasic rectangular current pulses (500 µA) at 1 kHz for over 1×10^8 cycles. The changes in impedance at different frequencies were characterized periodically. Apart from that, more than 1000 CV scanning cycles at 100 mV s^{-1} were also performed as electrochemical stress to assess the stability. The changes in CSC_c were characterized after different CV cycles.

Photothermal and Photoelectrochemical Measurements: An 808 nm near-infrared laser (Shanghai Connect Fiber Co., LTD.) was used as the light source to investigate the photothermal properties of the samples, while the temperature detection and thermal image recording were performed with the infrared thermal imager (SAT HM300). The influence of power density (0.25–2 W cm^{-2}) on the photothermal performance was also investigated. The photothermal stability was then studied after suffering from six repeated cycles of 5 min irradiation ON and 5 min OFF.

All photoelectrochemical performance was measured on the same three-electrode system, applying an Xenon lamp as the visible-light source. Chronoamperometry method was used for recording the photocurrent response of samples, after subtracting the baseline value. The photoelectrochemical stability was then studied after suffering from six repeated cycles of 50 s irradiation ON and 50 s OFF. Electrochemical activity, including CV and EIS measurements, with/without light irradiation was investigated in a 0.1 M KCl solution containing 10 mM $K_3Fe(CN)_6/K_4Fe(CN)_6$ mixtures. CV sweeps were obtained between potential limits of −0.2 and 0.6 V at a scan rate of 50 mV s^{-1}.

Finally, the MXene/PDA-modified electrodes were utilized as a proof of concept to demonstrate their applicability as photoelectrochemical biosensor devices.

Biocompatibility Study: All animal experiments were conducted in accordance with the guidelines of Shenzhen Institute of Advanced Technology at Chinese Academy of Sciences. This study was approved by the Institutional Animal Care and Use Committee of Shenzhen Institute of Advanced Technology at Chinese Academy of Sciences (SIAT-IACUC-20230918-YGS-ZHZX-ZT-ZT-A0899-04). Primary mouse neuron isolation and culture were performed as described below. Briefly, mouse brains were collected from P1–P3 neonatal C57BL/6J mice. After removing meninges and blood vessels, the mouse cortex was minced and dissociated by gentle mechanical disruption in 16.5U mL^{-1} papain for 15 min. The cell suspension was then neutralized by 30 mg mL^{-1} ovomucoid and filtered through a 100 µm strainer. The cell pellets were re-suspended in 30% percoll and centrifuged at 300 g for 15 min. The cell pellets were re-suspended in PBS containing 0.5% bovine serum albumin (BSA) and underwent negative selection with Neuron Isolation Kit (Miltenyi 130-115-390) according to the manufacturer's manual. The neuron derived underwent centrifugation at 300 g for 5 min and resuspended in neuron culture medium (Neural basal medium +2%B27 supplement+1% penicillin and strepcillin), then inoculated in 24-well plates for cell adhesion examination and 96-well plates for cell viability assay.

For the neuron adhesion assay, the purified neurons were cultured on the surface of different electrodes in a neuron culture medium for 24 h; the

neurons that remained adhered on different surfaces were fixed with 4% paraformaldehyde (PFA). The fixed neuron was permeabilized with 0.1% Triton-X100 and blocked with 5% bovine serum albumin (BSA), followed by immunostaining with an antibody against β-tubulin III(Sigma, Cat#: T2200) antibody to label the neuron and 4′,6-diamidino-2-phenylindole (DAPI).

A Cell Counting Kit-8 (CCK8) viability assay was performed to assay the effect of electrode extracts on neuron viability. Electrodes were sterilized by soaking them in 75% ethanol overnight, followed by UV radiation for 3 h. The sterile electrodes were immersed in a neuron culture medium for 48 h for extract collection. The collected extracts were co-cultured with neurons for 72 h, followed by a CCK8 viability test (MEDChemExpress, Cat#: HY-K0301). The CCK8 kit uses a water-soluble tetrazolium salt that produces an orange formazan dye upon bio-reduction in the presence of an electron carrier. The formazan product is soluble in the culture medium, and the amount of formazan produced is directly proportional to the number of living cells. The CCK8 assay was performed as instructed by the manufacturer.[52]

Supporting Information

Supporting Information is available from the Wiley Online Library or from the author.

Acknowledgements

This research was financially supported by the joint funding program of the Guangdong Department of Science and Technology and Hongkong Innovation and Technology Fund (2021A0505110015), Shenzhen Overseas Innovation Team Project, and the Science and Technology Innovation Council of Shenzhen (KQTD20170810105439418, KQTD20180413181834876 and JCYJ20200109114237902), and Joint Research Laboratory of SIAT-XZJ-HZD (E1Z149). The authors would like to thank Shiyanjia Lab (www.shiyanjia.com) for the support of AFM and TEM testing.

Conflict of Interest

The authors declare no conflict of interest.

Data Availability Statement

The data that support the findings of this study are available from the corresponding author upon reasonable request.

Keywords

bioelectronic interfaces, fast electrodeposition, MXene, neural electrodes, polydopamine (PDA)

Received: October 16, 2023
Revised: December 24, 2023
Published online:

[1] G. Balakrishnan, J. Song, C. Mou, C. J. Bettinger, *Adv. Mater.* **2022**, *34*, 2106787.
[2] Q. Zeng, Z. Huang, *Adv. Funct. Mater.* **2023**, *33*, 2301223.
[3] H. Yuk, J. Wu, X. Zhao, *Nat. Rev. Mater.* **2022**, *7*, 935.
[4] D. Ando, T. F. Teshima, F. Zurita, H. Peng, K. Ogura, K. Kondo, L. Weiß, A. Hirano-Iwata, M. Becherer, J. Alexander, B. Wolfrum, *J. Nanobiotechnol.* **2022**, *20*, 491.
[5] C. Kleber, K. Lienkamp, J. Rühe, M. Asplund, *Adv. Biosyst.* **2019**, *3*, 1900072.
[6] Q. Zeng, Z. Huang, G. Cai, T. Wu, *Adv. Mater. Interfaces* **2021**, *8*, 2100965.
[7] Q. Zeng, K. Xia, Y. Zhang, T. Wu, *Adv. Mater. Interfaces* **2019**, *6*, 1900356.
[8] Q. Zeng, K. Xia, B. Sun, Y. Yin, T. Wu, M. S. Humayun, *Electrochim. Acta* **2017**, *237*, 152.
[9] Q. Zeng, X. Li, S. Zhang, C. Deng, T. Wu, *Nano Select.* **2022**, *3*, 903.
[10] M. Zhu, H. Wang, S. Li, X. Liang, M. Zhang, X. Dai, Y. Zhang, *Adv. Healthcare Mater.* **2021**, *10*, 2100646.
[11] M. Alhabeb, K. Maleski, B. Anasori, P. Lelyukh, L. Clark, S. Sin, Y. Gogotsi, *Chem. Mater.* **2017**, *29*, 7633.
[12] A. Ahmed, M. M. Hossain, B. Adak, S. Mukhopadhyay, *Chem. Mater.* **2020**, *32*, 10296.
[13] P. K. Kalambate, N. S. Gadhari, X. Li, Z. Rao, S. T. Navale, Y. Shen, V. R. Patil, Y. Huang, *TrAC, Trends Anal. Chem.* **2019**, *120*, 115643.
[14] M. Rafiq, S. Rather, T. U. Wani, A. H. Rather, R. S. Khan, A. E. Khan, I. Hamid, H. A. Khan, A. S. Alhomida, F. A. Sheikh, *Chin. Chem. Lett.* **2023**, *34*, 108463.
[15] S. Panda, K. Deshmukh, S. K. Khadheer Pasha, J. Theerthagiri, S. Manickam, M. Y. Choi, *Coord. Chem. Rev.* **2022**, *462*, 214518.
[16] R. E. Ustad, S. S. Kundale, K. A. Rokade, S. L. Patil, V. D. Chavan, K. D. Kadam, H. S. Patil, S. P. Patil, R. K. Kamat, D. Kim, T. D. Dongale, *Nanoscale* **2023**, *15*, 9891.
[17] S. Aftab, M. Zahir Iqbal, S. Hussain, H. H. Hegazy, F. Kabir, S. Hassan Abbas Jaffery, G. Koyyada, *Chem. Eng. J.* **2023**, *469*, 144039.
[18] F. E. A. Latif, A. Numan, N. M. Mubarak, M. Khalid, E. C. Abdullah, N. A. Manaf, R. Walvekar, *Coord. Chem. Rev.* **2022**, *471*, 214755.
[19] X. Qu, Y. Guo, C. Xie, S. Li, Z. Liu, B. Lei, *ACS Nano* **2023**, *17*, 7229.
[20] Y. Yao, L. Lan, X. Liu, Y. Ying, J. Ping, *Biosens. Bioelectron.* **2020**, *148*, 111799.
[21] F. Zhao, Y. Yao, C. Jiang, Y. Shao, D. Barceló, Y. Ying, J. Ping, *J. Hazard. Mater.* **2020**, *384*, 121358.
[22] C. Jiang, X. Li, Y. Yao, L. Lan, Y. Shao, F. Zhao, Y. Ying, J. Ping, *Nano Energy* **2019**, *66*, 104121.
[23] C. Jiang, C. Wu, X. Li, Y. Yao, L. Lan, F. Zhao, Z. Ye, Y. Ying, J. Ping, *Nano Energy* **2019**, *59*, 268.
[24] N. Driscoll, B. Erickson, B. B. Murphy, A. G. Richardson, G. Robbins, N. V. Apollo, G. Mentzelopoulos, T. Mathis, K. Hantanasirisakul, P. Bagga, S. E. Gullbrand, M. Sergison, R. Reddy, J. A. Wolf, H. I. Chen, T. H. Lucas, T. R. Dillingham, K. A. Davis, Y. Gogotsi, J. D. Medaglia, F. Vitale, *Sci. Transl. Med.* **2021**, *13*, eabf8629.
[25] N. Driscoll, A. G. Richardson, K. Maleski, B. Anasori, O. Adewole, P. Lelyukh, L. Escobedo, D. K. Cullen, T. H. Lucas, Y. Gogotsi, *ACS Nano* **2018**, *12*, 10419.
[26] R. Zhou, B. Tu, D. Xia, H. He, Z. Cai, N. Gao, G. Chang, Y. He, *Anal. Chim. Acta* **2022**, *1201*, 339653.
[27] M. Herber, D. Lengle, S. R. Valandro, M. Wehrmeister, E. H. Hill, *Nano Lett.* **2023**, *23*, 6308.
[28] Y. Shao, L. Wei, X. Wu, C. Jiang, Y. Yao, B. Peng, H. Chen, J. Huangfu, Y. Ying, C. J. Zhang, J. Ping, *Nat. Commun.* **2022**, *13*, 3223.
[29] X. Jian, T. Li, S. Guo, L. Gao, F. Fu, Y. Tian, Y. Wu, *ACS Appl. Energy Mater.* **2022**, *5*, 3092.
[30] Y. Hu, S. Pang, G. Yang, X. Yao, C. Li, J. Jiang, Y. Li, *Mater. Res. Bull.* **2022**, *150*, 111761.
[31] Y. Cai, L. Zhang, R. Fang, Y. Wang, J. Wang, *Sep. Purif. Technol.* **2022**, *292*, 121019.
[32] Q. Zeng, W. Wan, L. Chen, *ACS Appl. Mater. Interfaces* **2019**, *11*, 24308.
[33] L. Yang, W. Zheng, P. Zhang, J. Chen, W. B. Tian, Y. M. Zhang, Z. M. Sun, *J. Electroanal. Chem.* **2018**, 830, *1*.
[34] J. Deng, Z. Lu, L. Ding, Z.-K. Li, Y. Wei, J. Caro, H. Wang, *Chem. Eng. J.* **2021**, *408*, 127806.

[35] Q. Zeng, S. Zhao, H. Yang, Y. Zhang, T. Wu, *Micromachines* **2019**, *10*, 419.
[36] S. Huang, Y. Fu, A. Mo, *Front. Chem.* **2022**, *10*, 1.
[37] F. Tian, J. Yu, W. Wang, D. Zhao, J. Cao, Q. Zhao, F. Wang, H. Yang, Z. Wu, J. Xu, B. Lu, *J. Colloid Interface Sci.* **2023**, *638*, 339.
[38] Z. Huang, Q. Zeng, Y. Hui, M. E. E. Alahi, S. Qin, T. Wu, *ACS Appl. Mater. Interfaces* **2020**, *12*, 14495.
[39] B. Wan, N. Liu, Z. Zhang, X. Fang, Y. Ding, H. Xiang, Y. He, M. Liu, X. Lin, J. Tang, Y. Li, B. Tang, G. Zhou, *Carbohydr. Polym.* **2023**, *314*, 120929.
[40] H. Wang, L. Li, C. Zhu, S. Lin, J. Wen, Q. Jin, X. Zhang, *J. Alloys Compd.* **2019**, *778*, 858.
[41] Z. Huang, Q. Zeng, S. Qin, T. Wu, *IEEE Sens. J.* **2021**, *21*, 22868.
[42] T. Marchesi D'Alvise, S. Harvey, L. Hueske, J. Szelwicka, L. Veith, T. P. J. Knowles, D. Kubiczek, C. Flaig, F. Port, K.-E. Gottschalk, F. Rosenau, B. Graczykowski, G. Fytas, F. S. Ruggeri, K. Wunderlich, T. Weil, *Adv. Funct. Mater.* **2020**, *30*, 2000378.
[43] H. Rastin, B. Zhang, A. Mazinani, K. Hassan, J. Bi, T. T. Tung, D. Losic, *Nanoscale* **2020**, *12*, 16069.
[44] S. Bai, X. Guo, T. Chen, Y. Zhang, X. Zhang, H. Yang, X. Zhao, *Composites, Part A* **2020**, *139*, 106088.
[45] J. Li, A. Levitt, N. Kurra, K. Juan, N. Noriega, X. Xiao, X. Wang, H. Wang, H. N. Alshareef, Y. Gogotsi, *Energy Storage Mater.* **2019**, *20*, 455.
[46] S. Chen, J. Xu, M. Shi, Y. Yu, Q. Xu, X. Duan, Y. Gao, L. Lu, *Appl. Surf. Sci.* **2021**, *570*, 151149.
[47] J. Wang, T. Dai, Y. Zhou, A. Mohamed, G. Yuan, H. Jia, *J. Colloid Interface Sci.* **2022**, *613*, 94.
[48] Y. Li, R. Fu, Z. Duan, C. Zhu, D. Fan, *ACS Nano* **2022**, *16*, 7486.
[49] J. Wang, D. Jiang, Y. Zhang, Y. Du, Y. Sun, M. Jiang, J. Xu, J. Liu, *J. Colloid Interface Sci.* **2024**, *653*, 229.
[50] B. Yan, M. Zhou, Y. Yu, B. Xu, L. Cui, Q. Wang, P. Wang, *Composites, Part A* **2022**, *160*, 107038.
[51] M. Ganji, A. C. Paulk, J. C. Yang, N. W. Vahidi, S. A. Dayeh, *Nano Lett.* **2019**, *19*, 6244.
[52] Q. Zeng, S. Yu, Z. Fan, Y. Huang, B. Song, T. Zhou, *Nanomaterials* **2022**, *12*, 3445.
[53] C. Chen, S. Ruan, X. Bai, C. Lin, C. Xie, I.-S. Lee, *Mater. Sci. Eng., C* **2019**, *103*, 109865.
[54] Y. H. Kim, G. H. Kim, A. Y. Kim, Y. H. Han, M.-A. Chung, S.-D. Jung, *J. Neural Eng.* **2015**, *12*, 066029.
[55] Q. Zeng, T. Wu, *J. Appl. Polym. Sci.* **2022**, *139*, 51804.
[56] L. Lu, X. Fu, Y. Liew, Y. Zhang, S. Zhao, Z. Xu, J. Zhao, D. Li, Q. Li, G. B. Stanley, X. Duan, *Nano Lett.* **2019**, *19*, 1577.
[57] Y. Wang, R. Garg, J. E. Hartung, A. Goad, D. A. Patel, F. Vitale, M. S. Gold, Y. Gogotsi, T. Cohen-Karni, *ACS Nano* **2021**, *15*, 14662.
[58] W.-T. Cao, W. Feng, Y.-Y. Jiang, C. Ma, Z.-F. Zhou, M.-G. Ma, Y. Chen, F. Chen, *Mater. Horiz.* **2019**, *6*, 1057.
[59] B. Xu, M. Zhu, W. Zhang, X. Zhen, Z. Pei, Q. Xue, C. Zhi, P. Shi, *Adv. Mater.* **2016**, *28*, 3333.
[60] C. Yuan, Z. He, Q. Chen, X. Wang, C. Zhai, M. Zhu, *Appl. Surf. Sci.* **2021**, *539*, 148241.
[61] L. Ling, C. Yuan, Q. Xu, T. Li, M. Zhu, C. Zhai, *Surf. Interfaces* **2023**, *36*, 102483.
[62] M. Ben Ali, H. Elhouichet, S. Szunerits, R. Boukherroub, *Chem. Eng. J.* **2022**, *450*, 138381.
[63] R. Yang, Q. Hu, S. Yang, Z. Zeng, H. Zhang, A. Cao, X. Gui, *ACS Appl. Mater. Interfaces* **2022**, *14*, 41997.
[64] Q. Yuan, Y. Liu, C. Ye, H. Sun, D. Dai, Q. Wei, G. Lai, T. Wu, A. Yu, L. Fu, K. W. A. Chee, C.-T. Lin, *Biosens. Bioelectron.* **2018**, *111*, 117.
[65] Y. Jiang, X. Xiao, C. Li, Y. Luo, S. Chen, G. Shi, K. Han, H. Gu, *Anal. Chem.* **2020**, *92*, 3981.
[66] Y. Zhong, Z. Wang, H. Liu, *Prog. Chem.* **2023**, *35*, 219.